Numerical modelling of grain refinement around highly reactive interfaces in processing of nanocrystallised multilayered metallic materials by duplex technique

Szymon Bajda[1], Dmytro Svyetlichnyy[1], Delphine Retraint[2] and Michal Krzyzanowski[1,3]*

[1] AGH University of Science and Technology, Faculty of Metals Engineering and Industrial Computer Science, Mickiewicza 30, Krakow 30-059, Poland.
[2] Institute Charles Delaunay, CNRS UMR 6281, LASMIS, University of Technology of Troyes, 10000 Troyes, France.
[3] Birmingham City University, Faculty Computing, Engineering & the Built Environment, Millennium Point, Curzon Street, Birmingham B4 7XG, UK

* Corresponding author. E-mail: michal.krzyzanowski@bcu.ac.uk; mkrzyzan@agh.edu.pl;

Abstract Microstructure evolution around highly reactive interfaces in processing of nanocrystallised multilayered metallic materials have been investigated and discussed in the present work. Conditions leading to grain refinement during co-rolling stage of the duplex processing technique are analysed using the multi-level finite element based numerical model combined with three-dimensional frontal cellular automata. The model was capable to simulate development of grain boundaries and changes of the boundary disorientation angle within the metal structure taking into account crystal plasticity formulation. Appearance of a large number of structural elements, identified as dislocation cells, sub-grains and new grains, has been identified within the metal structure as a result of metal flow disturbance and consequently inhomogeneous deformation around oxide islets at the interfaces during the co-rolling stage. These areas corresponded to the locations of shear bands observed experimentally using SEM-EBSD analysis. The obtained results illustrate a significant potential of the proposed modelling approach for quantitative analysis and optimisation of the highly refined non-homogeneous microstructures formed around the oxidised interfaces during processing of such laminated materials.

1. Introduction

Severe plastic deformation (SPD) leading to significant refining of the grain size is well known approach these days allowing for obtaining novel properties in metallic materials. The yield stress σ_y is strongly related to the grain size which is described by the Hall-Petch equation [1]:

$$\sigma_y = \sigma_0 + \frac{k}{\sqrt{d}} \quad (1)$$

where σ_0 is the grain interior resistant to deformation, k is the strengthening coefficient and d is the average grain diameter. Ghassemali et al. [2] recently showed that sub-grain formation together with specimen dimensions may also influence the mechanical respond of metals. Investigation has been also undertaken to evaluate an apparent grain size effect on the cell-substrate interactions in order to evaluate potential of these advanced materials to be applied as biomedical implants [3]. It is considered that absorption of proteins mediating the cell adhesion, enhancement of subsequent cell functioning and tissue growth can be altered by refining of the grain size to the nano-level [4]. Currently known SPD techniques, such as ECAE (Equal Channel Angular Extrusion), HPT (High Pressure Torsion), ARB (Accumulative Roll-Bonding) and SMAT (Surface Mechanical Attrition Treatment) usually allow for modification only of the surface layer of metallic materials. The usual thickness of the modified surface layer characterised by such significant grain refinement is not in excess of hundred microns [5, 6]. The small volume fraction of the refined to the nano-level grains within a structural metallic material is not sufficient for noticeable improvement of the bulk mechanical properties. To address this issue, the volume fraction of the ultrafine-grain structure within the material should be significantly increased.

Duplex techniques are attempted to be developed combining grain size refining processes based on SPD with a subsequent thermomechanical processing in order to produce multilayered bulk structures with improved yield and ultimate tensile strengths, while conserving an acceptable ductility measured as elongation to failure. Examples of such processes are shown in Fig. 1. Fig. 1a schematically illustrates angular accumulated drawing (AAD) process recently developed at AGH University of Science and Technology [7]. It is based on combining drawing, bending, burnishing, shearing and torsion. The main idea of the AAD process is to produce severe plastic deformation effects by applying a combination of inhomogeneous accumulation of work hardening effects. This method allows for obtaining severely refined microstructures distributed mainly at the surface layer of the metallic materials. SMAT technique is known for improvement of mechanical properties through formation of nanocrystallites at the surface layer (Fig 1b) [8]. The multistage drawing technique is used for production of steel magnesium composites in applications for which increased specific strength is required (Fig. 1c) [9]. Finally, the duplex technique based on combination of surface nanocrystallisation, generally known as SMAT, with subsequent rolling in order to produce multilayered bulk structures is presented (Fig. 1d) [10].

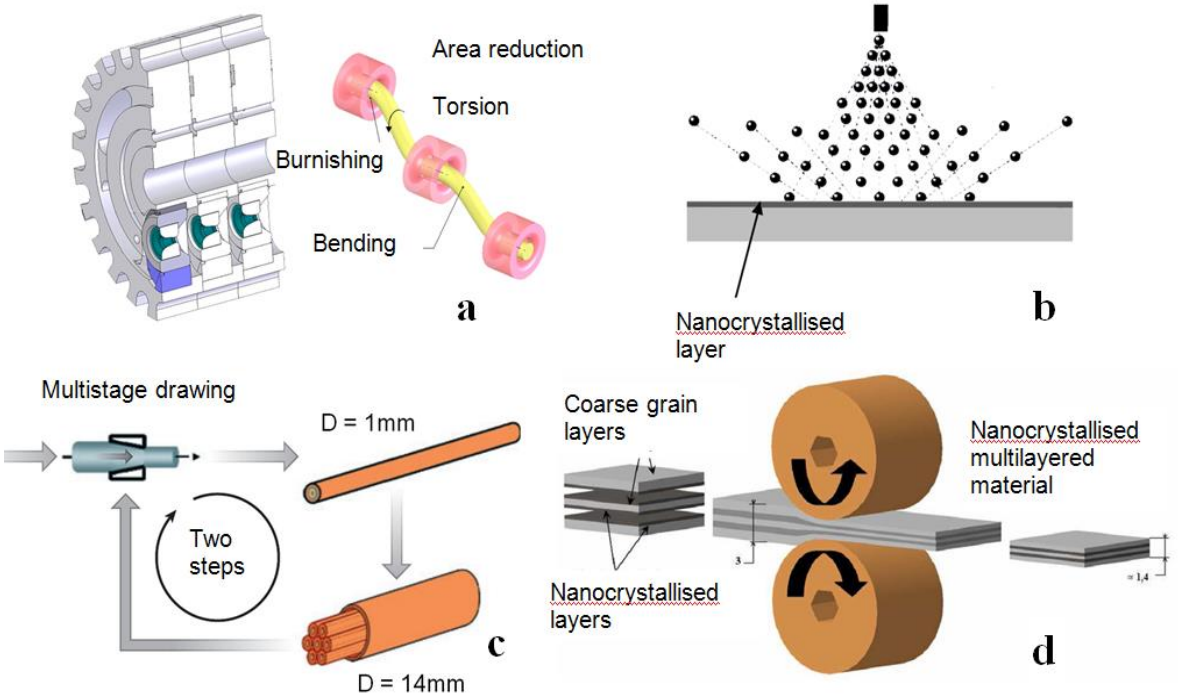

Fig 1 Schematic representation of the duplex technique components: a) angular accumulated drawing (AAD) [after 7], surface mechanical attrition treatment (SMAT) [after 8], multistage drawing [after 9] and subsequent rolling [after 10].

However, in duplex technique, the impurities deposited on the surface of the materials cause bonding imperfections due to interfacial oxidation during the rolling processing stage at high temperatures. As a consequence, either the oxide islets or continuous oxide layers are formed at the interfaces [11]. The interface oxidation occurring during duplex processes can influence the microstructure development around the interfaces depending on whether the oxide scale is a continuous layer or a layer of discontinuous oxide clusters with heterogeneous thicknesses. Effectively, the oxide scale becomes a part of the microstructure development of

such nano-crystallised multilayered structures. Shear banding has been observed near metal-metal contact between the oxide clusters at the interfaces [12]. The shear banding can be considered as some kind of bonding enhancement creating channels for the base metal of the different laminates to come into contact through the oxidised interface. The similar phenomenon was also observed in roll-bonding of aluminium alloys at high temperatures [13], where the difference in mechanical properties of oxides and metal and also dimensions of the oxide fragments have been recognised as important technological factors. As it was shown elsewhere [14], the greater the difference in hardness, the higher the probability of shear banding formation across the oxidised interface. Temperature, texture and grain size were also mentioned by the same authors among other factors influencing the shear banding. The behaviour of the highly reactive interfaces during the processing of nanocrystallised multi-layered materials has recently been investigated numerically using the developed multi-level thermomechanically coupled finite element (FE) based model [15]. The macro-level part of the model representing the multilayered nanocrystallised metallic material has been linked to the meso-level part representing the oxidised interface within the material. The results of the analysis supported the possibility of strain localisations formed around the oxide islets at the interface between nanocrystallised fcc 316L austenitic stainless steel plates during the hot rolling stage of the duplex processing technique. The similar deformation zones after the hot rolling stage did not appear near continuous oxide layers. They also have not been noticed in the vicinity of the deliberately imbedded oxide fragments during the modelling trials favouring the conclusion that the initially continuous oxide layers failed during the rolling pass because of their lower ductility at 550^{o}C than the one for nanocrystallised metal.

A computer modelling of microstructure evolution around the oxide clusters during co-thermomechanical processing is fraught with difficulties mainly due to a lack of proper numerical tools allowing representation of the dislocation structures making prediction at micro- and meso-level a great challenge. Modelling approaches based on cellular automata (CA) seems occupy the first place among the numerical methods applicable to quantitative analysis of microstructure evolution. CA based modelling is currently used for analysis of crystallization (solidification) [16 – 20], dynamic and static recrystallization [21 – 28], phase transformation [23, 29] and also grain refinement [30 – 38]. Usually, these are simple and relatively fast two-dimensional (2D) models consisting of a few elements and connections. They are much simpler for designing, implementation and easier for visualization. However, at least five main problems are left partly unresolved in such simplified 2D approaches, among of them are kinetics of transformation, location of nuclei, grain growth rate, deformation of grains and crystallographic orientation. 3D CA are free of these problems, however, they are more complex and require much more time and memory for simulations. One of the possible modifications, known as frontal cellular automata (FCA) approach, allowing for significant reduction of the calculation time, is used in this paper. Conception of FCA was described by the authors in details elsewhere along with a simplified model not taking into consideration a real deformation process [30]. The CA models were developed progressively distributing the effects of deformation on slip planes and slip directions according to the crystal plasticity theory [31, 32]. They have been applied for modelling of accumulative roll-bonding (ARB) [33] and MaxStrain technology [37]. Then later, the CA model has been effectively applied for analysis of microstructure evolution in different combined metal forming processes consisting of accumulative angular drawing, multi-pass linear wire drawing and wire flattening designed for obtaining ultrafine-grained microstructure [38].

The objective of this work is to understand the evolution of microstructure around the oxidised interfaces during the consecutive rolling stage of the duplex processing on the basis of the advanced multi-level numerical analysis supported by experimental studies of the grain refinement. In the simulations, the meso-level of the previously developed multi-level FE based model is combined

with the state-of-the-art 3D FCA numerical model allowing for both the appearance of new boundaries and rotation of dislocation cells (sub-grains and grains) simultaneously.

2. Multi-level numerical modelling

Oxidation inevitably takes place between different metallic laminates at the interfaces during subsequent rolling at elevated temperatures. A detailed multi-level FE based numerical investigation supported the possibility of strain localisations formed around the oxide islets at the interface between nanocrystallised fcc 316L austenitic stainless steel plates during the subsequent rolling stage of the duplex processing technique, the effect earlier noticed experimentally [11, 15]. It favoured the conclusion that the scale failed during the rolling pass having lower ductility than the underlying nanocrystallised metal at the relatively low temperatures, up to 550^{o}C. It has been shown that the rolling reduction of 45% was not sufficient for significant extrusion of nanocrystallised metal into the voids between fragmented oxide scale leaving unfilled gaps between the steel plates of the laminate causing bonding imperfections at the laminate interfaces during the processing. The voids around 20μm thick scale fragments can remain unclosed during the rolling even at 55% rolling reduction posing additional risk of damage within the transition layers near the sides of the elongated oxide clusters. Although the developed model was advanced enough to be able to include into analysis few micrometre thick scale clusters, voids and complicated profile of the interface, it did not reflect all physical phenomena taking place at the oxidised interfaces, particularly it did not consider microstructure evolution around the interfaces of the steel laminate as part of the mentioned co-operative relationships. For this reason, the meso-component of the multi-level FE model described in details earlier [15] has been linked to the FCA based model capable to simulate the microstructural changes during plastic deformation taking into account crystal plasticity formulation (Fig. 2).

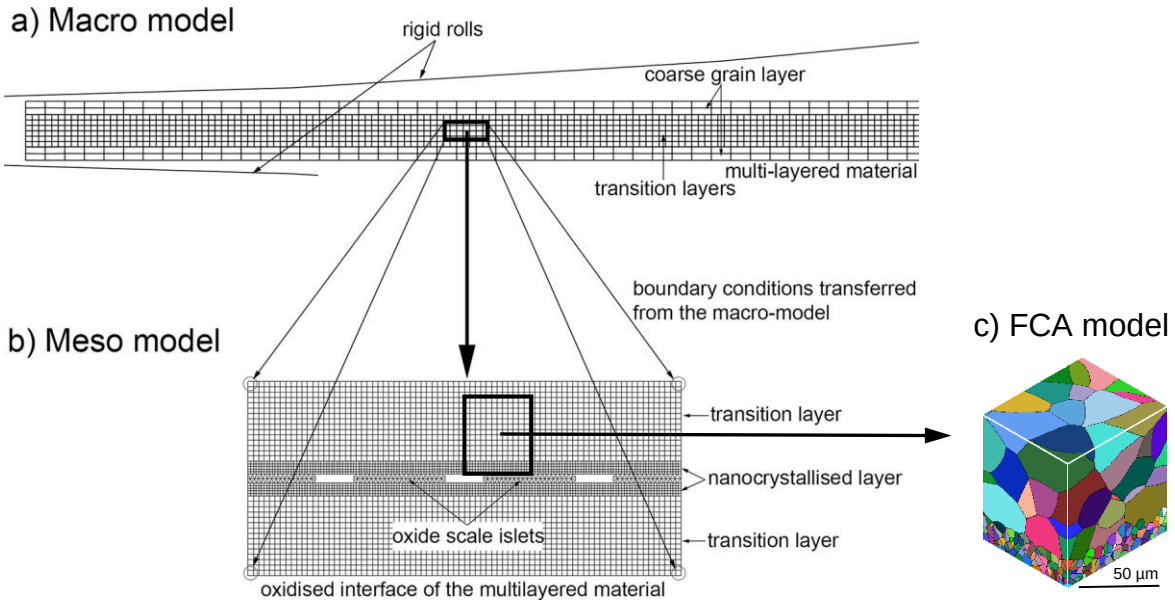

Fig. 2. Scheme of combined FE/FCA based multi-level model setup

The multi-level modelling setup used in the work is composed of three following models: macro- and meso- both FE based models and FCA model linked together. The macro- and meso- FE based models are rigorously thermo-mechanically coupled within the Abaqus/Standard commercial software. The strains are confined to the plain contacting surface normal to the rolling direction in this 2D FE approach that can be assumed for rolling of the

relatively thin plates. The approach allows for calculation of the distribution of velocities, strains, strain rates, stresses and temperature around the oxidised interface in the middle part of the specimen. All parameters used in the FE calculations were introduced on the basis of the available experimental data and are summarised elsewhere [15]. They include the thermal and mechanical properties of the coarse grain, transition and nanocrystalline layers for the corresponding three layers of the 316L stainless steel, the heat loss to the environment through convection and radiation, the heat loss due to conduction to the rolls, the heat generated during deformation of the rolled material and the relevant friction coefficients between the roll and steel surfaces. The stress-strain curve representing the constitutive behaviour of each layer has been assumed as a function of the equivalent strain $\bar{\boldsymbol{\varepsilon}}$ and the temperature T (Table 1). The rolls were assumed to be rigid bodies. The macro-level model setup consisted of 8800 CPE4RT elements representing two plates undergoing flat rolling. Each plate included both the coarse grain and the transition layer. The macro-level model allowed for calculation of strains, strain rates, stresses and temperatures in the middle part of the specimen. The field variables from the macro- model were transferred to the meso-level model as boundary conditions. The meso-level model setup included nanocrystallised layers consisted of 9600 CPE4T elements and also oxide scale fragments consisted of 292 CPE3T elements. The dimensions of the oxide scale fragments were assumed to be similar to those observed experimentally, about 30– 120 μm in length and 10–20 μm in thickness. They were assumed to be adherent to the metal surface when the clearance between two contacted surfaces becomes zero. The possibility of viscous sliding between the scale fragments and the metal surface arising from the shear stress during the deformation was assumed in the modelling in an analogous manner to grain-boundary sliding in high-temperature creep. The calculation of the viscosity coefficient was based on a microscopic model for stress directed diffusion around irregularities at the interface depending on the temperature, the volume diffusion coefficient and the diffusion coefficient for metal atoms along the oxide metal interface and the interface roughness parameters.

Table 1 The stress-strain curves representing the constitutive behaviour of the corresponding layers of the 316L stainless steel applied for the modelling [15].

Layer:	**Flow stress:**
Coarse grain	$\bar{\sigma}_c = 335 + 1255\,\bar{\varepsilon}^{0.733} - 0.095\,T^{1.1}$
Transition	$\bar{\sigma}_t = 775 + 481\,\bar{\varepsilon}^{0.502} - 0.095\,T^{1.1}$
Nanocrystalline	$\bar{\sigma}_n = 1803 + 338\,\bar{\varepsilon}^{0.0712} - 0.095\,T^{1.1}$

3. FCA model of grain refinement

The 3D FCA model used in this work has been described in details elsewhere [30, 32, 36] and is only briefly summarised here. The model of grain refinement uses two different CA. The first one presents spatial discretization of the representative volume. In the case under consideration, cellular space of 600×320×320 cells represents volume of 75×64×81 μm^3. The cells belong to the corresponding grain having appropriate properties. Some of the properties are associated with the cells, others related to the grains. Dislocation density is not associated with the cells. All cells have the same shape and size and are changed uniformly. Grain refinement is modelled including the following two stages, namely: formation of new boundaries and rotation of structural elements. The grains are considered in the second CA model, where every grain, sub-grain and dislocation cell has their own structure of CAs. The grain model of 316L austenitic stainless steel, having fcc crystal structure and 12 slip systems,

is represented by twelve one-dimensional (1D) CAs while number of cells in the 1D CA depends on the resolution and grain size in the appropriate direction. It is crucial in the analysis of nanocrystalline materials to be able modelling the evolution of dislocation density and substructure arrangement. The evolution of dislocation density is calculated for every cell and is based on crystal plasticity modelling approach, where the effects of deformation are caused by dislocation motion on active slip systems and by distortion of the crystal lattice. The designed 1D CAs use the information from the crystal plasticity module simulating generation and growth of the dislocation substructure. Corresponding crystallographic orientation of each grain gives basis for determination of the active slip systems. Growth of dislocation density leads to appearing of low-angle boundaries (LAB) when the density reaches its critical value. The LAB divides the grain into dislocation cells. Although the dislocation cells inherit CA model from their parent grain, they are considered independently in further analysis. The dislocation structure evolves at different rates due to differences in the slip rate for the different slip directions. The formed structure containing the dislocation cells is considered as an initial state for modelling of rotation of the dislocation cells, sub-grains and grains during subsequent straining.

The material spin of a polycrystalline material is the sum of the plastic spin and the lattice spin. It is defined as the skew-symmetric tensor obtained by decomposing the prescribed velocity gradient in a rotation and a deformation component:

$$W = W^p + W^l, \tag{2}$$

where W^p is the plastic spin and W^l is the lattice spin representing macroscopic rotation also called the constitutive spin or the rotation rate of the Mandel-frame. It is assumed that the plastic spin could be related to the rate of slip in slip systems of the lattice:

$$W^p = \sum_s \dot{\gamma}^s P_{ij}^s, \tag{3}$$

where $\dot{\gamma}^s$ is the glide velocity for the active slip system s, and P_{ij}^s is the skew part of the Schmid tensor defined by the slip plane and the slip direction.

3.1. Data transfer from FEM to FCA

From various sets of the rolling process parameters applied in the FE modelling, one set was selected to illustrate the capabilities of the FCA calculations. To ensure compliance with the results obtained in the experimental studies, the set selected for the simulation contains the process parameters identical to those applied in the real rolling process allowing for obtaining multilayered nanocrystallised metallic material with discontinuous oxide scale islets. Thus, the initial temperature of 550 °C and 55% rolling reduction were selected for the FCA modelling. The oxide scale thickness was assumed to be 10 μm in correspondence to the results of microscopic observations. The data from FE calculations were transferred for CA simulations using several files. Each file is assumed to contain records of a calculation step for the number of nodes corresponding to the chosen area of the FE mesh. The quantitative information about the whole deformation process is divided into six consecutive stages corresponding to the different time moments and is saved in six files. The consecutive stages correspond to six different time moments of the deformation during the rolling pass and can be expressed as the percentage of progress, namely 0, 37, 50, 62, 75 and 100%. The files contain the nodal coordinates, three components of the strain tensor and the effective strain. The regular rectangular FE mesh allowed for easier adaptation of the obtained FE data for the following FCA modelling. The FE mesh was progressively refined toward the oxidised interface in the applied model. The finest mesh was assumed in the area near the oxide scale, where grains of the metallic structure are expected to be smaller while the strains in the area supposed to be

higher. Thus, the domain with fine and coarse 2D mesh, as it is shown in Fig. 3, has been transferred to 3D FCA model, which had initially uniform cells.

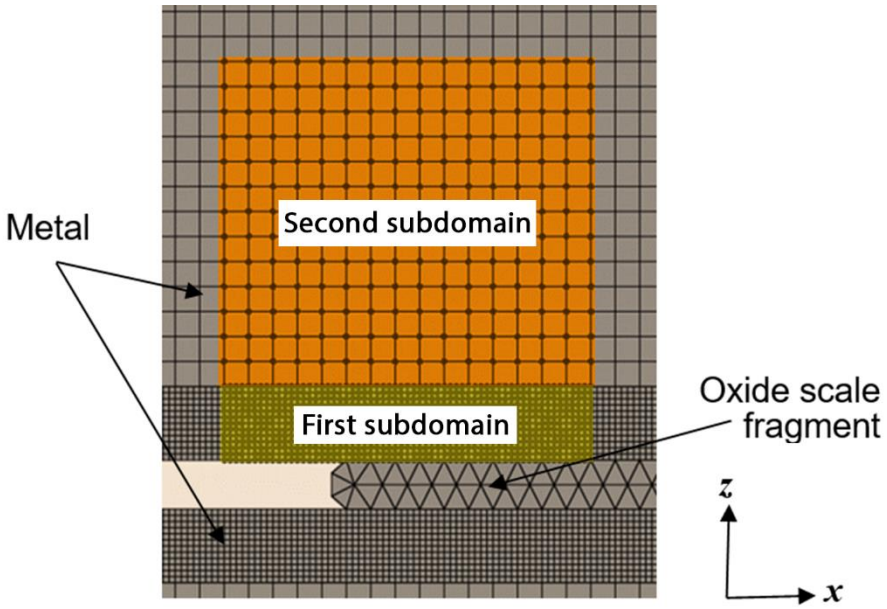

Fig. 3. Highlighted nodes of the FE meso model domain situated around the oxidised interface containing information used for FCA modelling

The size of the FE domain transferred for FCA simulation was $x \times z$ = 75 μm ×80 μm and it contained two subdomains. The first subdomain containing 60×12 square elements with the side length of 1.25 μm covered the area of 75×15 μm^2 and the second one containing 15×13 square elements with the side length of 5 μm covering the area of 75×65 μm^2 around the laminate interface. The following 3D CA was developed basing on this data with the geometrical sizes of $x \times y \times z$ = 75 μm ×64 μm ×80 μm. The third dimension y of the CA was chosen taking into account the average size d of the coarse grains at the beginning of the process, in such way that $y = 3 \div 4\ d$. There were total $n_x \times n_y \times n_z$ = 600×320×320 = 61 440 000 cells created, where n_x, n_y and n_z are the corresponding numbers of cells in x, y and z direction. The corresponding initial sizes of the cells are $c_x \times c_y \times c_z$ = 0.125 μm ×0.2 μm ×0.25 μm. The choice of the cell sizes is a compromise between a desirable resolution and a number of the cells, i.e. between the accuracy of fine grains representation, the memory capacity and the computational time. Therefore, each square element of the first FE subdomain has been transformed into 3D substructure with 10×320×5 cells, while 40×320×20 cells represented each element of the second subdomain. Such substructures remain rigidly connected with the corresponding finite element. Nodal coordinates of the element define corresponding coordinates of the cells with two-linear interpolation, and also the components of the strain tensor and the effective strain for every cell. Therefore, every cell within the x-z cross-section is of unique shape with the associated strain tensor and the effective strain during and after the deformation. At the same time, they have the same shape in y direction with the corresponding strain tensor and the effective strain. Such transfer of the coordinates from FEM to FCA allows for obtaining the same shapes and sizes in this two methods. On the other hand, due to high isotropic behaviour of the applied algorithm, the calculation method used in FCA allows for elimination of the cell shape and size influence on the modelling results.

3.2. Initial microstructure

The study is devoted to the microstructure evolution during the second stage of the duplex process. Modelling of microstructure evolution begins from development of a representative initial microstructure. The initial microstructure observed at the surface layer of the steel sample after the SMAT process is presented in Fig. 4. It has to be noted that the microstructure presented further in the text both from using EBSD orientation maps and figures representing the results of FCA simulations are coloured according to Inverse Pole Figure (IPF). The two areas with significant difference in the grain size can be observed at the presented cross-section of the steel sample subjected to SMAT. The area with very fine grains can be observed at the surface of the sample while the second one, where much coarser grains with signs of twins are observed, is situated deeper inside the specimen. The boundary between the mentioned two areas is distinctly visible. However, there is almost no visible transient zone between them. The representative not homogeneous initial microstructure developed in the FCA model should reflect all the mentioned important peculiarities of the real microstructure while omitting less important details. It is not a common task and the development requires implementation of additional to the standard methodology procedures described elsewhere [39]. Periodic boundary conditions, commonly applied in CA simulations of microstructure evolution, cannot be applied when deformation and grain size are not uniform. Generally, such conditions can only be applicable along one direction, for instance along *y* axis, while the grain size in any other direction should be somewhat reduced to eliminate a boundary effect on the grain size.

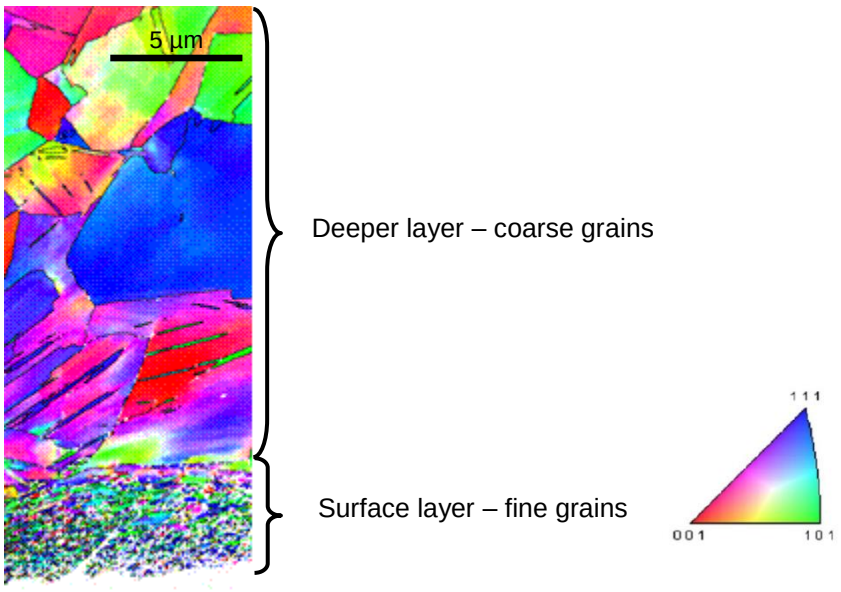

Fig. 4. Image of the initial microstructure obtained using EBSD technique at the cross section of 316L steel sample after SMAT coloured according to Inverse Pole Figure (IPF).

The algorithm for the initial microstructure development has been modified in this study to take into account parameters of the real not homogeneous microstructure observed at the surface layer of the samples after SMAT. The microstructure is modelled using nucleation and free grain growth. Taking into account that the grain size depends on the nucleation process, mainly on a number of nuclei in a volume unit, the probability of nucleon appearance has been assumed as a function of the desirable grain size in this location. This function contains three components, each component reflects one coordinate dependence. The dependence on *x* and *y* coordinates compensate the boundary effect. The dependence on *z* coordinate (along the thickness) divides the modelling space additionally on three domains with different grain sizes.

The average grain size was about 12 μm in the first domain and about 3 μm in the last one while the middle domain played a role of the transition area between them. Preliminary computations, however, exhibited that the introduction of the appropriate nucleation function is not enough for development of the initial microstructure, and some corrections to the grain growth algorithm were necessary. First of all, the grain growth rate has been made dependent on the desirable grain size. Then, the grain growth rate was additionally decreased after the grain reached the desirable size. It has to be noticed that even such rigorous correction of the grain growth algorithm did not allow obtaining smooth transition between the two areas with significant difference in grain size.

The initial 3D microstructure representation reflecting the main peculiarities of the real structure observed using EBSD investigations is presented in Fig. 5. Comparison of the modelled initial microstructure with the real one observed after the SMAT shows some differences, which were recognized as acceptable for the purpose of the modelling. The main part of the 3D representative cell has the microstructure very similar to the real one in connection with both size and shape of the grains. However, the modelled grain structure has no twins and it is more homogeneous with regard to the internal crystallographic orientation. The surface of modelled structure is plane and continuous. The grains situated in the surface part of the layer and characterized with fine grain sizes are generally coarser in the model than in the real material. It is connected with resolution of the model where some margin has been deliberately assumed for possible further refinement during deformation in the consecutive rolling stage. Such an assumption can be considered as reasonable because the grain size considered in the FCA simulation has no feedback on the properties and character of the material flow during the deformation. In addition, obtaining plain border between two areas with different grain sizes is fraught with difficulties.

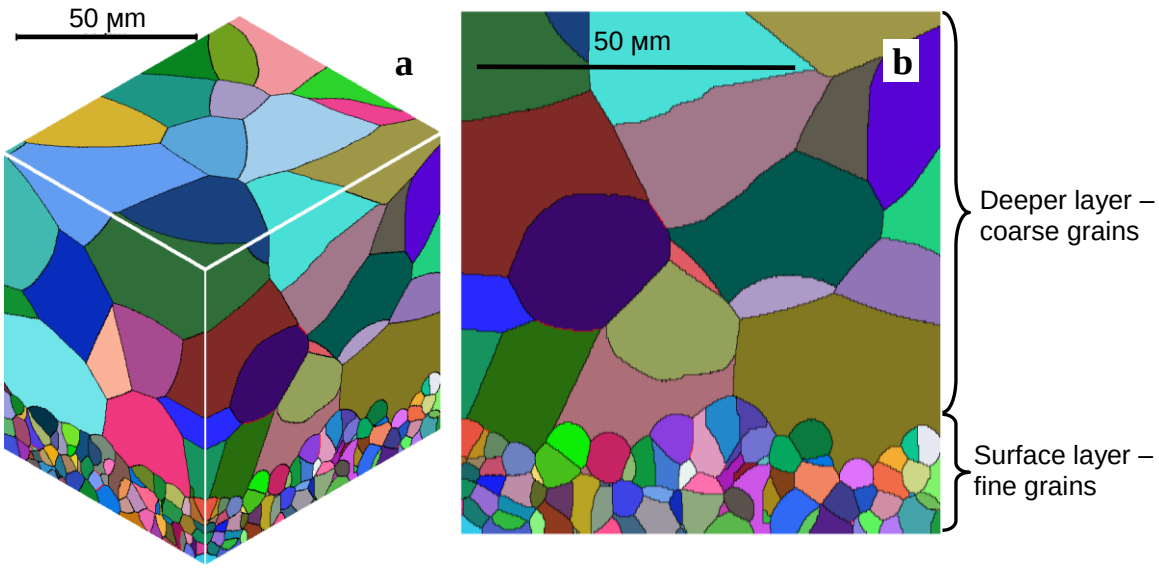

Fig. 5. Initial microstructure developed for FCA modelling, a – isometric view; b – x-z plane.

3.3. Grain refinement

Grain refinement is modelled by considering both formation of the new boundaries and rotation of the structural elements (grains). Formation of the new boundaries is modelled in the following way. First, the active slip systems are determined for each grain (crystal) based on the grain orientation and the strain tensor. Then, the strain is decomposed on the slip fraction for the active slip systems. The appeared low-angle boundaries (LAB) divide the grain into several sub- regions, such as dislocation cells. They inherit CA model from the parent grain and they are considered as independent structural elements. Every new LAB divides an old grain on two structural elements. Because the slip rate is different for the different slip directions and the different grain orientation, both appearance and evolution of the structural elements progress at different rates. Firstly, LABs appear in one slip direction. Then, they appear in other directions.

Dislocation density changes in each cell of 1D CA with the strain fraction and this is the product of two components: deterministic and stochastic. The deterministic component describes evolution of the dislocation density as hardening and dynamic recovery while the stochastic component is represented by the normal distribution with a small dispersion.

In the earlier modelling approach described elsewhere [33], the cells changed their state and new LABs appeared during the deformation when the dislocation density in the cell walls reached a critical value. The cells in a LAB have an influence on their neighbourhood. Considering the deformation mechanism as movement of dislocations, LABs act as barriers for the movement. Thus, all dislocations move toward or away from the LABs. Positive feedback occurs in the LAB cell and all its neighbours when the new LAB cell appears. The dislocation density of the LAB cells increases because of this positive feedback that causes an increase of the strain hardening. At the same time, the dislocation density decreases very fast in all neighbouring cells. In the later developments [40, 41], instead of a critical value of the dislocation density, the new boundaries with the highest dislocation density chosen from all 1D CA determine appearance of the new LAB. In this approach, the number of the new boundaries is defined by the equation, which determines an expected grain size. Such an approach proved to be significantly more stable than the one based on an introduction of the

constant critical value allowing for better controlled solution. In the model, four variables were proposed for consideration of the effects of strain on appearance of the new dislocation cells [36]. Although such an approach is useful for modelling of grain refinement during uniform strain deformation, it fails when the grain size and the strain are not uniform. Moreover, any influence of the size of the refined grains on the refinement rate are not considered.

In the present study, it is assumed that the grain size during the severe deformation is inversely proportional to square root of the strain ($d \sim \varepsilon^{-0.5}$). Hence, by application of the incremental calculations, the following dependence can be obtained for calculation of the current desirable grain size d:

$$d = \begin{cases} \sqrt{\dfrac{ad_0}{\varepsilon_{ac}}} & \forall d \geq d_{\min} \\ d_{\min} & \forall d < d_{\min} \end{cases}, \tag{4}$$

where d_0 is the initial or current grain size before deformation, ε_{ac} is the accumulative effective strain and a is the adjusted material coefficient, which can be treated as a coefficient of proportionality for the considered material. The coefficient sets a rate of the grain refinement. The minimal grain size $d_{\min}$ has been added because of both the cell resolution and natural limitations of grain refinement in materials posing a restriction on the grain size that can be obtained in the model. In spite of divisions on smaller substructures, rotation of the structural elements is also considered in the simulation. The rotation is defined by the crystallographic orientation and depends on the applied deformation. It is assumed that the structural elements are rotated by a small randomly defined angle, which is represented by following equation [39, 40]:

$$\Delta\vartheta = \vartheta_0 r \Delta\varepsilon, \tag{5}$$

where $\Delta\vartheta$ is the rotation angle, ϑ_0 is the rotation factor (it can be a function of the strain), r is a randomly chosen number from the uniform distribution within the range of [-1,1] and $\Delta\varepsilon$ is the effective strain increment. The rotation factor ϑ_0 can be a function of the strain. It introduces the scale or the rate of grains rotations and defines how quickly the microstructure reaches its final state of grain boundary misorientations. The rotations change grain boundary misorientation angles while the grain boundary misorientation angle in its turn defines whether the structural element is treated as a dislocation cell, a sub-grain or a grain.

1. Results of CA simulation

The minimal grain size $d_{\min}$, the rotation factor ϑ_0 and the coefficient a were changed in the study of grain refinement during the consecutive rolling stage of the duplex processing. The modelling results corresponding to the following three data sets of the above mentioned parameters are presented in this section to demonstrate their influence on the final microstructure:

1) a = 2.5 μm, $d_{\min}$ = 0.5 μm, $\vartheta_0 = 2.0^o$
2) a = 1.5 μm, $d_{\min}$ = 0.4 μm, $\vartheta_0 = 2.0^o$ (6)
3) a = 0.75 μm, $d_{\min}$ = 0.4 μm, $\vartheta_0 = 4.0^o$

As indicated previously, the quantitative information about the whole deformation process has been divided into the five consecutive stages. The results of CA modelling obtained for the set 3 are presented in Fig. 6 – 8. They are the closest to the available experimental data. The initially created microstructure with randomly orientated grains includes only grains

separated by the high angle boundaries (HAB). Then, consecutive deformation stages were simulated. Deformation of the initial microstructure and the first signs of appearance of new LABs can be observed at the end of the first stage (Fig. 6). The appeared LABs are scarcely presented and can be noticeable mainly in the case of the data set 3. The LABs separate grains into clusters that can be considered as dislocation cells. The model does not explicitly distinguish the structural elements, such as grains, sub-grains or dislocation cells. However, they can be determined on the basis of a mis-orientation angle between CA cells.

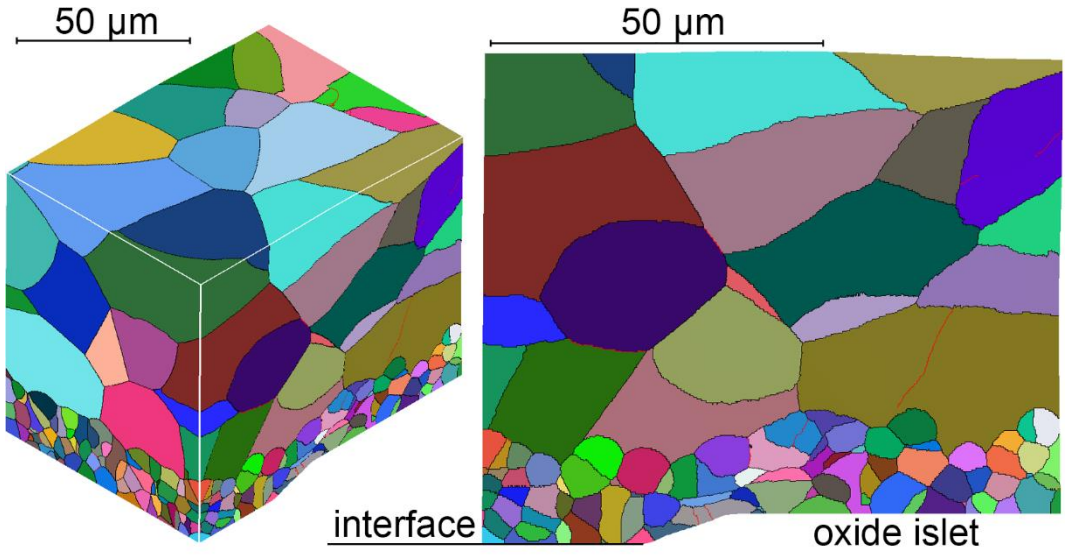

Fig. 6. Microstructure of 316L steel around oxidised interface predicted after the first stage of deformation during co-rolling (isometric view – *left*; x-z plane – *right*; data set 3).

After the consecutive deformation stages, the number of appeared LABs increases. The maximum frequency of the LAB appearance remains nearly the same while a rotation rate is relatively small. Then, the rotation of CA cells influences an increase of the boundary mis-orientation angle resulting in their gradual transformation into the sub-grains (Fig. 7). Further rotation during deformation leads to additional increase of the mis-orientation angles. As a result of such microstructure evolution, the first LABs have been transformed into HABs after the fourth deformation stage (Fig. 7e, f). Such rotation of the new dislocation cells leads to changes in their crystallographic orientation. It can be noticeable in Fig. 7c, d representing the predicted microstructure of the material around the oxidised interface after the third stage of deformation, where the colour scheme reflects the Euler angles describing the grain orientation.

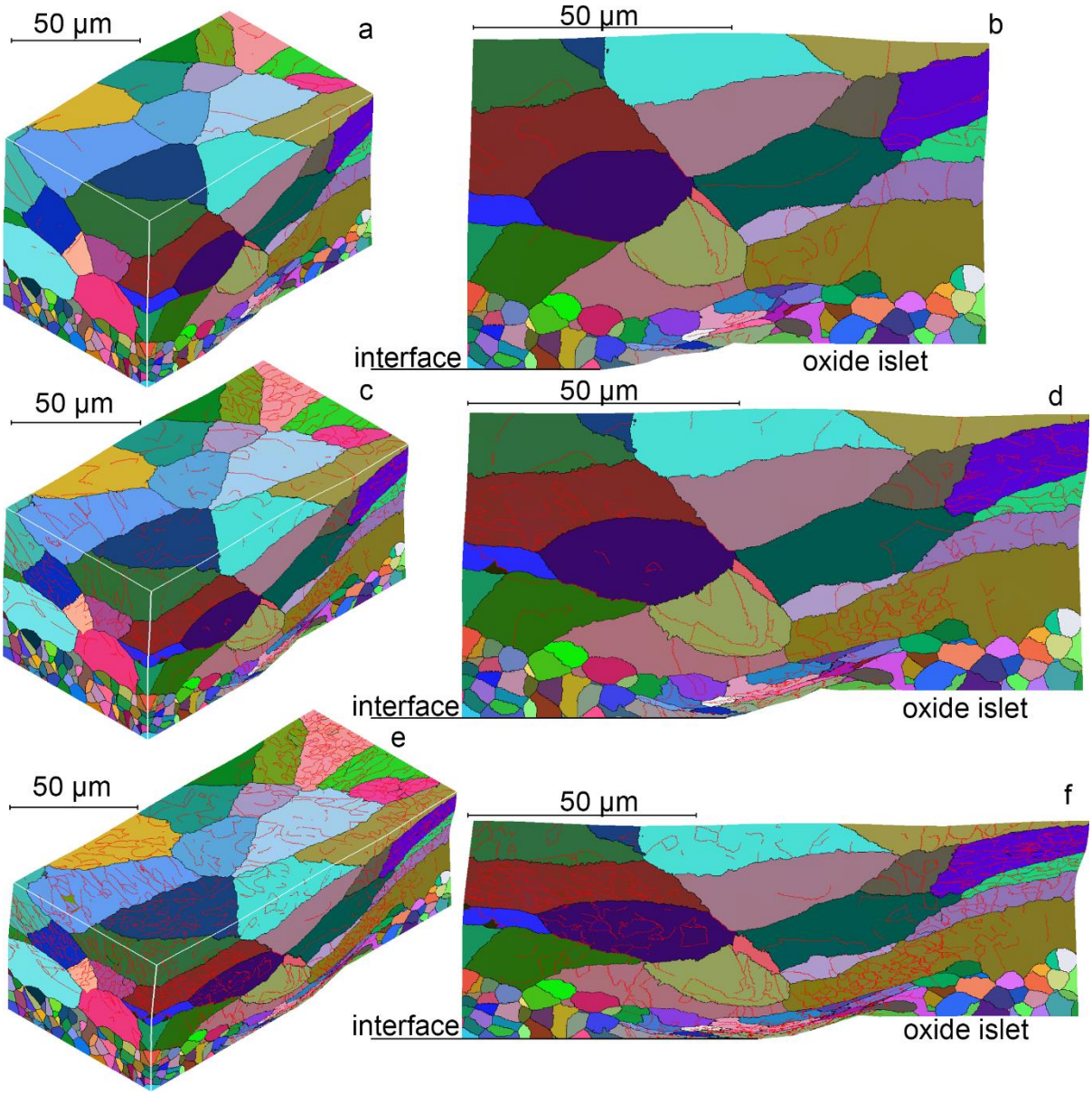

Fig. 7. Microstructure of 316L steel around oxidised interface predicted after the second (a, b), third (c, d) and fourth (e, f) consecutive stages of deformation during co-rolling (a, c, e – isometric view; b, d, f – x-z plane; data set 3).

Comparing the results obtained for the mentioned above three data sets applied in the FCA modelling, it can be noticed that in spite of some similarities, the minimal grain size d_{min}, the rotation factor ϑ_0 and the coefficient a play a significant role in grain refinement during the consecutive rolling stage of the duplex processing (Fig. 8 and 11). The amount of LABs predicted for the chosen data sets during such deformation is much lower for data set 1 corresponding to higher coefficient a (Fig. 8a, b). The decreasing of minimal final grain size d_{min} and the coefficient a (data set 2) allows for obtaining finer final microstructure (Fig. 8c, d). A further decrease in the coefficient a coupled with doubling of the rotation factor $\vartheta_{0,}$ corresponding to the parameters from data set 3, resulted in faster development of the refined microstructure (Fig. 8e, f). For all parameter data sets, the predicted LABs and HABs were

accumulated in the areas corresponding to the locations of the shear bands between the oxides observed experimentally.

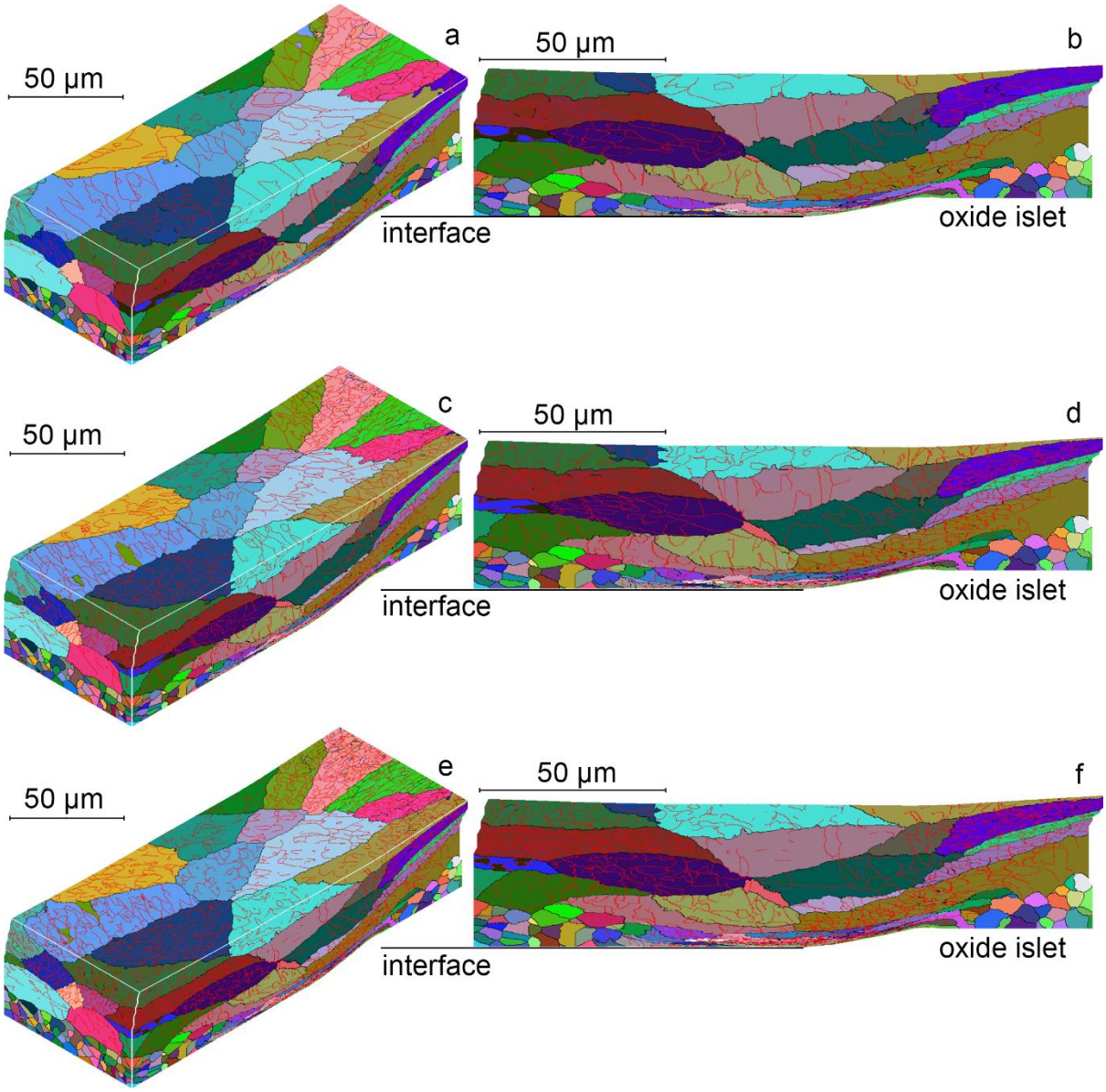

Fig. 8. Microstructure of 316L steel around oxidised interface after the last stage of deformation during co-rolling predicted for data set 1 (a, b), data set 2 (c, d) and data set 3 (e, f). (a, c, e –isometric view; b, d, f – x-z plane).

It is assumed in the developed FE model that the oxide islets situated at the interfaces of the metallic laminate have lower ductility than the adjacent metallic layers. They almost retain their shape during such deformation presenting an obstacle to metal flow during rolling. As a consequence, highly inhomogeneous deformation takes place leading to formation of strain localisations and inhomogeneous microstructure in these areas (Fig. 6 – 8). The zones of strain localisation start at the sides of oxide islets spreading further around the islets. As it was observed experimentally, shear bands can be present in such zones around the oxide fragments, indicated by letters A and C in Fig. 9a, c. Similar zones characterised by high density of

boundaries can also be identified using the obtained modelling results (Fig. 9b – letters A and C). Moreover, it has been shown both experimentally and numerically, that the coarse grains initially observed well above the oxidised interfaces between the scale fragments retain their sizes after the rolling operation practically without newly formed LABs (letter B in Fig. 9a, b). Similarly, the initially fine grains response differently to the applied inhomogeneous deformation depending on the area. The fine grains situated near the interface between the scale fragments are highly deformed during the rolling operation and characterised by the extensively changed shape (letters A in Fig. 9b), while the grains located immediately above the middle of the scale fragment change their size insignificantly and are characterised with appearance of the newly formed LABs (letter D in Fig. 9b).

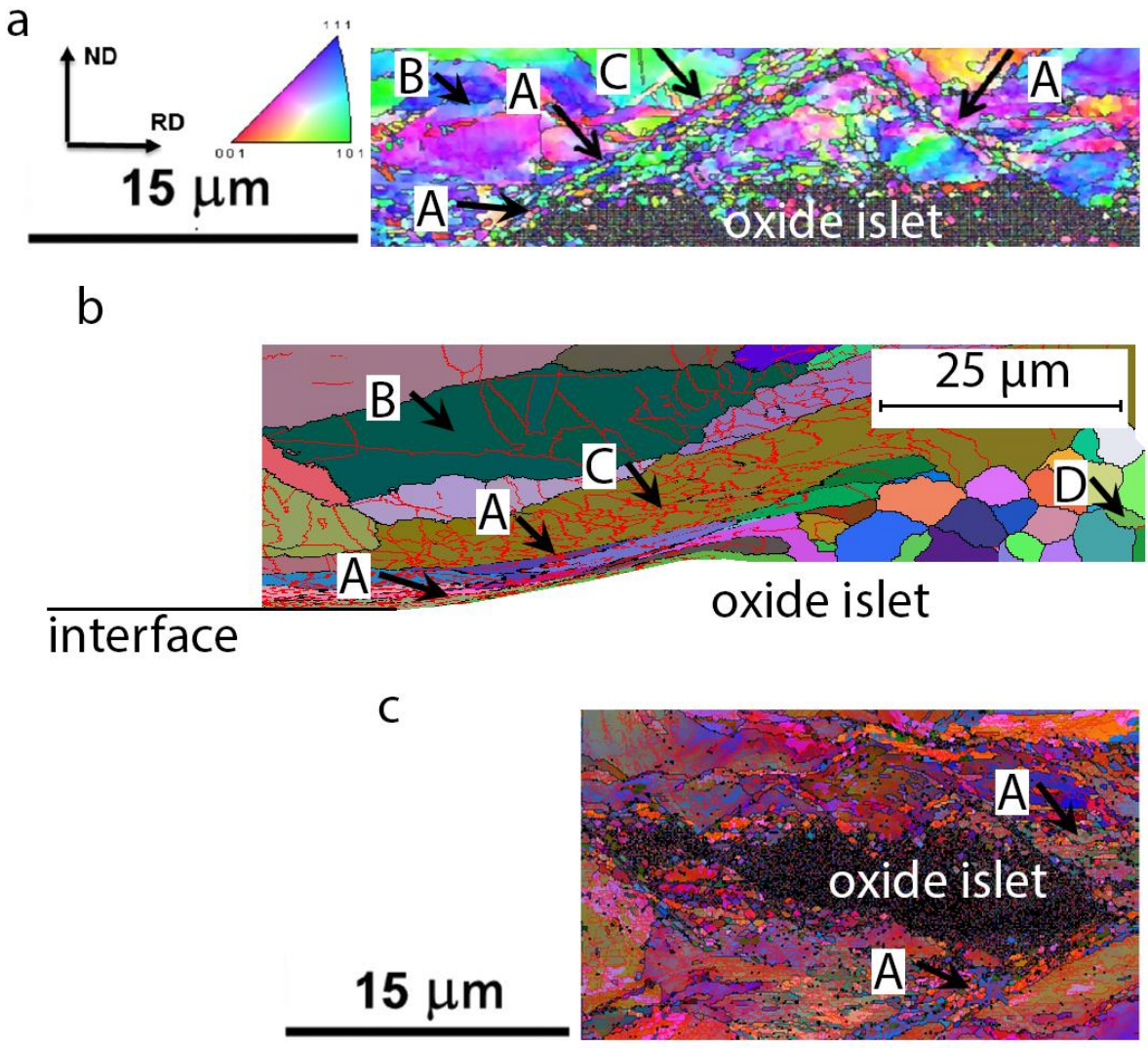

Fig. 9. EBSD orientation map of the cross-section area near the oxide islets after co-rolling coloured according to Inverse Pole Figure (IPF) (**a**) and Euler angles (**c**) compared with obtained modelling results (**b**). Arrows A and C indicate shear bands and refined grains, arrow B – coarse grains, arrow D - newly formed LABs ; **b, c** - HABs (black) and LABs (red) are shown.

As it has been shown above, the grain refinement in the FCA modelling is controlled by the set of three parameters, namely the minimal grain size d_{min}, the rotation factor ϑ_0 and the coefficient a (eq. 6). They influence number of the newly appeared grain boundaries and

structural elements (Fig. 10a), and also average size of the structural elements (Fig. 10b). However, the values obtained are averages and they do not reflect inhomogeneity of the final structure. For example, average sizes of the structural elements calculated assuming date set 3 for the areas A-D, shown in Fig. 9b, are respectively the following: A – 0.6, B – 9.8, C – 1.1, D – 2.6 μm, while the average size calculated for the whole representative volume is 1.3 μm.

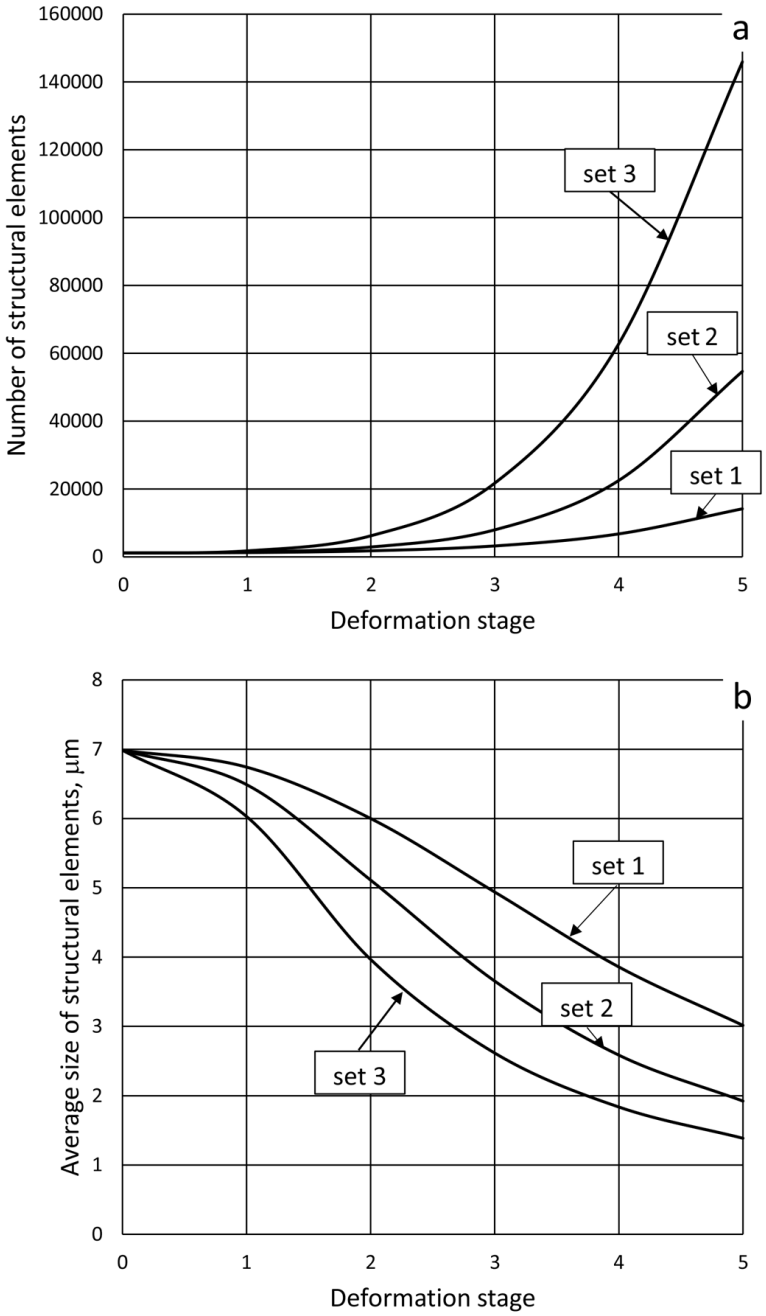

Fig. 10. The total number of the structural elements including dislocation cells, sub-grains and new grains (a) and the their average size (b) predicted during co-rolling assuming three data sets of the FCA model parameters (eq. 6)

As it can be seen from Fig. 11 illustrating distribution of the grain boundary disorientation angle predicted for the different stages of the co-rolling process, only HABs can be identified within the steel structure before the rolling operation. At the beginning of the deformation, a small amount of new LABs appeared. Their formation significantly

increases in the second part of the rolling process, particularly during stages 4 and 5, which results from strain accumulation within steel matrix around the oxide islets. At the same time, the amount of HABs increased slightly.

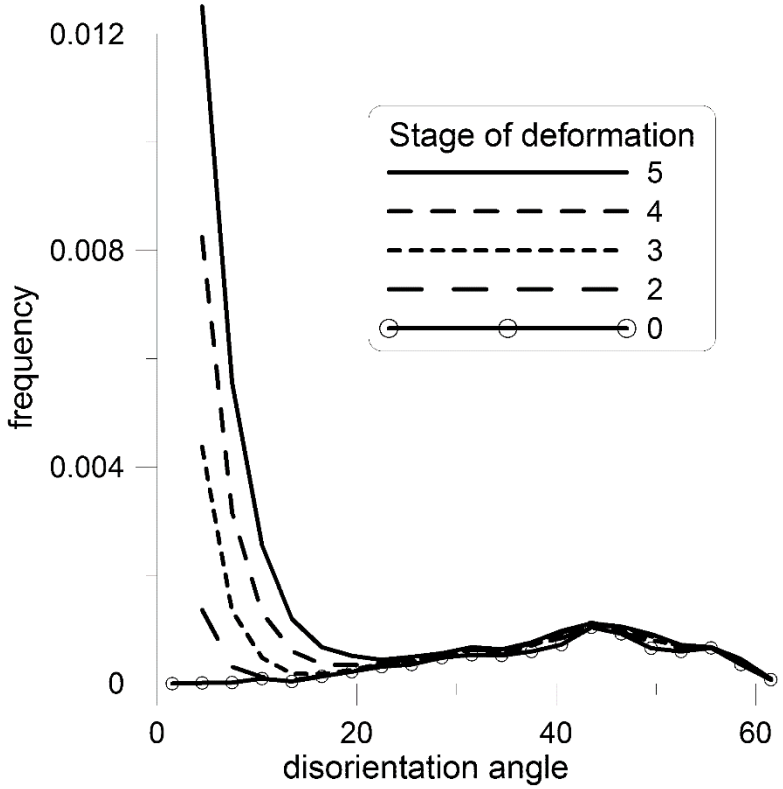

Fig. 11 Distribution of the grain boundary disorientation angle predicted during different stages of the co-rolling process assuming data set 3 (eq. 6) of the FCA model parameters.

Summary

The application of the multi-level FE based model coupled with three-dimensional FCA for the grain refinement simulation is discussed in the paper. The presented results are related to microstructure evolution of 316L austenitic stainless steel around highly reactive interfaces in the co-rolling stage of the duplex technique applied for processing of nanocrystallised multilayered metallic materials. The FCA part of the model is capable to simulate development of grain boundaries and disorientation angles within the metal structure during plastic deformation taking into account crystal plasticity formulation.

The results of the numerical analysis supported by the experimental evidence showed the large number of structural elements appeared in the zones around oxide islets at the interfaces during co-rolling. The appearance of the structural elements, identified as dislocation cells, sub-grains and new grains, was due to metal flow disturbance and consequently inhomogeneous deformation. These areas corresponded to the locations of shear bands observed experimentally. It has been shown that the number of the appeared structural elements increases for higher rotation factor ϑ_0, lower final minimal grain size $d_{\min}$ and lower coefficient a. The mentioned parameters define grain refinement in the FCA model. The number of the structural elements significantly rises at the end of the rolling stage. The amount of LABs in the areas around interfaces increased notably comparing to the amount of the identified HABs.

The proposed multi-level model that consists of three parts offers an effective numerical tool for prediction of the microstructure evolution around the oxidised interfaces during processing of the laminated metallic materials for different structural applications**.** A reasonably good agreement achieved between the modelling results and the results of SEM-EBSD analysis illustrates a significant potential of the proposed modelling approach for quantitative analysis and optimisation of the highly refined non-homogeneous microstructures formed around the oxidised interfaces during the processing route. The modelling approach opens up new research opportunities toward improvement of its predictive accuracy, such as including more accurate consideration of strain localisation taking into account appearance of twins, shear and micro- bands allowing extension of its applicability to other materials.

Acknowledgements:

The support from the National Science Centre, Poland (grant no. DEC-2013/09/B/ST8/00141) is greatly appreciated.

References:

1. E. Arzt, Size effects in materials due to microstructural and dimensional constraints: a comparative review, Acta Materialia, Vol. 46, 1998, 5611-5626.
2. E. Ghassemali, M. Tan, C.B. Wah, S.C.V. Lim, A.E.W. Jarfors, Effect of cold-work on the Hall–Petch breakdown in copper based micro-components, Mechanics of Materials, Vol. 80, 2015, 124-135.
3. S. Bagherifard, R. Ghelichi, A. Khademhosseini, M. Guagliano, Cell response to nanocrystallized metallic substrates obtained through severe plastic deformation, ACS Appl. Mater. Interfaces 6, 2014, 7963–7985;
4. T.J. Webster, C. Ergun, R.H. Doremus, R.W. Siegel, R. Bizios, Specific proteins mediate enhanced osteoblast adhesion on nanophase ceramics, J. Biomed. Mater. Res. 51, 2000, 475–483;
5. N.R. Tao, J. Lu, K. Lu, Surface nanocrystallization by surface mechanical attrition treatment, Mater. Sci. Forum 579, 2008, 91–108;
6. G. Liu, J. Lu, K. Lu, Surface nanocrystallization of 316L stainless steel induced by ultrasonic shot peening, Mater. Sci. Eng. A286, 2000, 91–95;
7. K. Muszka, L. Madej and Janusz Majta, The effects of deformation and microstructure inhomogeneities in the Accumulative Angular Drawing (AAD), Materials Science & Engineering A 574, 2013, 68-74.
8. B. Arifvianto, Dr Suyitno, M. Mahardika, Effects of surface mechanical attrition treatment (SAMT) on a rough surface of AISI 316L stainless steel, Applied Surface Science 258 (10), 2012, 4538-4543;
9. Embury D., Bouaziz O., Steel-based composites: Driving forces and classifications, Annu. Rev. Mater. Res., 40, 2010, 213.
10. L. Waltz, D. Retraint, A. Roos, C. Garnier, P. Olier, Effect of interfacial oxidation occurring during the duplex process combining surface nanocrystallisation and co-rolling, Surf. Coat. Technol. 205, 2011, 4608–4613;
11. L. Waltz, D. Retraint, A. Roos, C. Garnier, P. Olier, Effect of interfacial oxidation occurring during the duplex process combining surface nanocrystallisation and co-rolling, Surf. Coat. Technol. 205, 2011, 4608–4613;
12. D. Retraint, Z. Quadir, W. Xu, L. Waltz and M. Ferry, Microstructural investigation of co-rolled nanocrystalline stainless steel sheets, Materials Science Forum, 702-703, 2011, 127-130.

13. M.Z. Quadir, A. Wolz, M. Hoffman, M. Ferry, Influence of processing parameters on the bond toughness of roll-bonded aluminium strip, Scripta Mater. 52, 2005, 1039-1044.
14. M.Z. Quadir, M. Ferry, O. Al-Buhamad, P.R. Munroe, Shear banding and recrystallization texture development in a multi-layered Al ally sheet produced by accumulative roll bonding, Acta Mater. 57, 2009, 29-40.
15. S. Bajda, M. Krzyzanowski, K. Muszka, W.M. Rainforth, Numerical Analysis of highly reactive interfaces in processing of nanocrystallised multilayered metallic materials by using duplex technique, Surf. Coat. Technol. 277, 2015, 170-180.
16. M. Rappaz, C.-A. Gandin, Probabilistic modeling of microstructure formation in solidification processes, Acta Metall. Mater. 41, 1993, 345-360.
17. D. Raabe, Mesoscale simulation of spherulite growth during polymercrystallization by use of a cellular automaton, Acta Mater. 52, 2004, 2653-2664.
18. A.A. Burbelko, E. Fraś, W. Kapturkiewicz, D. Gurgul, Modelling of dendritic growth during unidirectional solidification by the method of cellular automata, Mater. Sci. Forum, 649, 2010, 217-222.
19. A. Burbelko, D. Gurgul, E. Guzik, W. Kapturkiewicz, Cellular automaton simulation for volume changes of solidifying modular cast iron, Archives of Metallurgy and Materials, Vol. 60, Issue 3, 2015, 2379-2384.
20. D.S. Svyetlichnyy, Modelling of macrostructure formation during the solidification by using frontal cellular automata, in: A. Salcido (Ed.), Cellular automata - Innovative modelling for science and engineering, In Tech, Croatia, 2011, 179-196, doi: 10.5772/15773.
21. H.W. Li, XX Sun, H Yang, A three-dimensional cellular automata-crystal plasticity finite element model for predicting the multiscale interaction among heterogeneous deformation, DRX microstructural evolution and mechanical responses in titanium alloys, International Journal of Plasticity, Vol. 87, 2016, 154-180.
22. M. Qian, Z.X. Guo, Cellular automata simulation of microstructural evolution during dynamic recrystallization of an HY-100 steel, Mater. Sci. Eng., A 365, 2004, 180-185.
23. M. Kumar, R. Sasikumar, P. Kesavan Nair, Competition between nucleation and early growth of ferrite from austenite – studies using cellular automation simulations, Acta Mater., 46, 1998, 6291-6303.
24. D.S. Svyetlichnyy, Modelling of the microstructure: from classical cellular automata approach to the frontal one, Comput. Mater. Sci., 50, 2010, 92-97.
25. F. Chen, K. Qi, Z.S. Cui, X.M. Lai, Modelling the dynamic recrystallization in austenitic stainless steel using cellular automaton method, Comput. Mater. Sci., 83 2014, 331-340.
26. O. Beltran, K. Huang, R. E. Loge, A mean field model of dynamic and post-dynamic recrystallization predicting kinetics, grain size and flow stress, Comput. Mater. Sci., Vol. 102, 2015, 293-303.
27. W.F. Shen, LW. Zhang, C. Zhang, Y.F. Xu, X.H. Shi, Constitutive Analysis of Dynamic Recrystallization and Flow Behavior of a Medium Carbon Nb-V Microalloyed Steel, Journal of Materials Engineering and Performance, Vol. 25, Issue 5, 2016, 2065-2073.
28. P. Asadi, M.K.B. Givi, M. Akbari, Simulation of dynamic recrystallization process during friction stir welding of AZ91 magnesium alloy, International Journal of Advanced Manufacturing Technology, Vol. 83, Issue 1-4, 2016, 301-311.
29. P. Macioł, J. Gawąd, R. Kuziak, M. Pietrzyk, Internal variable and cellular automata-finite element models of heat treatment, Int. J. Multiscale Comp. Eng. 8, 2010, 267-285.

30. D.S. Svyetlichnyy, Simulation of microstructure evolution during shape rolling with the use of frontal cellular automata, ISIJ Int. 52, 2012, 559–568.
31. K.J. Song, Y.H. Wei, Z.B. Dong, X.H. Zhan, W.J. Zheng, K. Fang, Numerical simulation of beta to alpha phase transformation in heat affected zone during welding of TA15 alloy, Comput. Mater. Sci., 72, 2013, 93-100.
32. D.S. Svyetlichnyy, Three-dimensional frontal cellular automata model of microstructure evolution – phase transformation module, ISIJ Int. 54, 2014, 1386-1395.
33. D. Svyetlichnyy, J. Majta, K. Muszka, Modelling of microstructure evolution of BCC metals subjected to severe plastic deformation, Steel Res. Int. 79, 2008, 452-458.
34. D.S. Svyetlichnyy, Modelling of microstructure evolution in process with severe plastic deformation by cellular automata, Mater. Sci. Forum, 638-642, 2010, 2772-2777.
35. D. Svyetlichnyy, J. Majta, K. Muszka, Ł. Łach, Modelling of microstructure evolution of BCC metals subjected to severe plastic deformation, AIP Conf. Proc. 1315, 2010, 1473-1478.
36. D.S. Svyetlichnyy, Simulation of grain refinement by cellular automata, Comp. Mater. Sci. 77, 2013, 408-416.
37. Y. Liu, Q. Zeng, Z. Feng, L. Cheng, L. Li, L. Zhang, Numerical Analysis of the Microstructure-based Model for Layered Composites via MC and FEM Approaches, Brazilian Journal of Physics, Vol. 46, Issue: 1, 2016, 87-96.
38. A. Wierzba, S. Mroz, P. Szota, A. Stefanik, R. Mola, The influence of the asymmetric ARB process on the properties of Al-Mg-Al multilayer sheets, Archives of Metallurgy and Materials, Vol. 60, Issue 4, 2015, 2821-2825.
39. D.S. Svyetlichnyy, A three-dimensional frontal cellular automaton model for simulation of microstructure evolution-initial microstructure module, Modelling and simulation in materials science and engineering, Vol. 22, Issue 8, Article Number: 085001, 2014.
40. D.S. Svyetlichnyy, K. Muszka, J. Majta, Three-dimensional frontal cellular automata modeling of the grain refinement during severe plastic deformation of microalloyed steel, Computational Materials Science, Vol. 102, 2015, 159-166.
41. J. Majta, Ł. Madej, D.S. Svyetlichnyy, K. Perzyński, M. Kwiecień, K. Muszka, Modeling of the inhomogeneity of grain refinement during combined metal forming process by finite element and cellular automata methods, Materials Science and Engineering A – Structural Materials Properties Microstructure and Processing, Vol. 671, 2016, 204-213.